Enhanced near-ambient temperature energy storage and electrocaloric effect in the lead-free BaTi0.89Sn0.11O3 ceramic synthesized by sol–gel method

Marwa Zahid, Youness Hadouch, M'barek Amjoud, Daoud Mezzane, Mohamed Gouné, Khalid Hoummada, Abdelhadi Alimoussa, Anna G. Razumnaya, Brigita Rožič, Zdravko Kutnjak

Enhanced near-ambient temperature energy storage and electrocaloric effect in the lead-free $BaTi_{0.89}Sn_{0.11}O_3$ ceramic synthesized by sol–gel method

Marwa Zahid[1*], Youness Hadouch[1,2] , M'barek Amjoud[1], Daoud Mezzane[1,2], Mohamed Gouné[3], Khalid Hoummada[4], Abdelhadi Alimoussa[1], Anna G.Razumnaya[5], Brigita Rožič[6] and Zdravko Kutnjak[6]

1. IMED-Lab, Cadi-Ayyad University, FST, Marrakech, Morocco.

2.LPMC, University of Picardie Jules Verne,

3. ICMCB, University of Bordeaux, Pessac, 33600, France

4. IM2NP, Aix Marseille University, Marseille, 13397, France

5. Faculty of Physics, Southern Federal University, Rostov-on-Don, 344090, Russia

6. Jožef Stefan Institute, Jamova Cesta 39, 1000 Ljubljana, Slovenia.

*Corresponding author:

E-mail: marwaz996@gmail.com; marwa.zahid@ced.uca.ma

ORCID: https://orcid.org/0000-0001-5676-3224

Abstract

Lead-free perovskite materials with high performance have high potential in clean energy storage applications and developments of electrocaloric devices. In this work, we report structural, dielectric, ferroelectric properties, energy storage and electrocaloric effectnear the ambient temperature in barium stannate titanate ($BaTi_{0.89}Sn_{0.11}O_3$, BTS_{11}) ceramic prepared by a sol-gel method. The formation of a single perovskite structure was confirmed using the X-ray diffraction analysis. An average grain size of 18.5µm was found by the mean of the SEM micrograph with a density of 5.91 g/cm^3.The presence of the multiphase at very near ambient temperature was proved using temperature-dependent micro-Raman measurements and differential scanning calorimetry. The BTS_{11} ceramic exhibits a high dielectric constant of 15460and a low dielectric loss (<0.055) with considerable temperature stability. Moreover, a high energy storage density of 122mJ/cm^{3}was showed with an efficiency of 79%, and a maximum value of ECE (ΔT) of 0.86 K and finally, an electrocaloric responsivity ($\Delta T/\Delta E$) of 0.24 K.mm/kV under the external electricfield of 35 kV/cm near ambient temperature. The enhanced dielectric, ferroelectric and electrocaloric properties in BTS_{11} ceramic makes it a great potential candidate for its uses in solid-state cooling technology and high-energy storage applications near ambient temperature.

Keywords: Lead-free, sol-gel process, energy storage, electrocaloric effect, ambient temperature, barium stannate titanate.

Declarations

Funding

This work was supported by CNRST Priority Program PPR 15/2015, by the European Union's Horizon 2020 research and Innovation actions MSCA-RISE-ENGIMA (No. 778072) and MSCA-RISEMELON (No. 872631) and ARRS project J1-9147, and by the ministry of Science and Higher Education of the Russian Federation, grant agreement No 075-15-2021-953.

Conflicts of interest/Competing interests

Not applicable

Availability of data and material

Not applicable

Code availability

Not applicable

Ethics approval

Not applicable

Consent to participate

We confirm that all authors mentioned in the manuscript have participated in, read and approved the manuscript and have given their consent for the submission and subsequent publication of the manuscript.

Consent for publication

We confirm that all the authors mentioned in the manuscript have agreed to publish this paper.

Relevance Summary

In the submitted manuscript, I am reporting, the successful synthesis of barium stannate titanate ceramics by sol-gel method, and the study of their structural, dielectric, ferroelectric, energy storage, and electrocaloric properties. In addition, we confirm that this work is original and has not been published elsewhere, nor is currently under consideration for publication elsewhere.

Acknowledgments

The authors gratefully acknowledge the generous financial support of the European Union Horizon 2020 Research and Innovation actions MSCA-RISE-ENGIMA (No. 778072) and MSCA-RISE-MELON (No. 872631) and ARRS project J1-9147 and program P1-0125 and CNRST Priority Program PPR 15/2015 and the ministry of Science and Higher Education of the Russian Federation, grant agreement No 075-15-2021-953.

1. Introduction:

Earlier studies and applications using ferroelectric properties of perovskite structural materials were carried out with lead-based materials such as lead-titanium zirconate (PZT)[1] and magnesium niobate-lead-titanate (PMN-PT)[2]. Unfortunately, due to lead toxicity[3], these lead-based materials can be harmful to the environment or human health, hence the need to develop clean and environmentally friendly lead-free material with improved ferroelectric properties.

Barium titanate (BaTiO3, BT) and its derivatives were the first lead-free perovskite materials studied and used for dielectric capacitors since 1950 [4]. These materials are eco-friendly and can be used to develop new lead-free materials with high piezoelectric, electrocaloric and energy storage properties[5].When doped with isovalent cations, the electrical and dielectric properties of BT tend to improve. Many systems have been studied over the

years, including the BCZT ($Ba_{0.85}Ca_{0.15}Ti_{0.9}Zr_{0.1}O_3$) system, which consists of calcium cation substitution on the A site and zirconium cation substitution on the B site [6],and BST ($Ba_{1-x}Sr_xTiO_3$) where the strontium is doped in the A site [7].The BTS ($BaTi_{1-x}Sn_xO_3$) system, on the other hand, is designed by inserting tin cations Sn^{4+} in the B site[5],[8],[9],[10]. Nonetheless, most of these materials tend to achieve significant energy storage and electrocaloric properties only around the Curie temperature when the ferroelectric to paraelectric transition occurs, i.e. in a narrow temperature range, limiting their applications. The emphasis is primarily on lead-free materials with diffuse phase transition that leads to a wider temperature range near ambient temperature, where the energy storage and the electrocaloric properties are improved [11].

In this regard, the Curie temperature has been reported to decrease from 120°C for the undoped BT system, to 40°C, 41°C and 37°C in the BTS systems[5,9,12]. As a result of the coexistence of the four phases, cubic, tetragonal, orthorhombic, and rhombohedral (R, O, T, and C) at the quadruple point near the ambient temperature (AT), defined as 25 °C by the International Union of Pure and Applied Chemistry (IUPAC), the BTS_{11} could achieve an extremely high dielectric constant, a high piezoelectric coefficient, enhanced energy storage, and a significant electrocaloric effect [9]. However, the dielectric peak remained noticeably sharp in all studied compositions. Gao et al. [12] conducted the study of the $Ba(Ti_{1-x}Sn_x)O_3$ ferroelectric material system with various compositions, and came to the conclusion that one aspect that requires to be addressed further is the poor temperature stability of the BTS system properties.

The most commonly used method for elaborating dense and performant BTS ceramics is the solid-state method, which produces non-homogeneously doped powders with a high risk of contamination and agglomeration, it also necessitates a high calcination temperature (1250 °C) [8]. However, the sol-gel method, which is also commonly used in thin film synthesis [13][14][15][16], is a simple and precise method that can produce a more uniform and fine powder with better stoichiometry control, resulting in improved dielectric and ferroelectric properties. and it also requires lower heating temperatures [17].

In the present study, structural, dielectric, ferroelectric and electrocaloric properties were investigatedin $BaTi_{0.89}Sn_{0.11}O_3$ceramic (BTS_{11}) and found to be enhanced around ambient temperature in a broad temperature range. Therefore, the BTS_{11}ceramic can be a suitable candidate for ambient temperature energy storage and frigorific applications.

2. Experimental details:

2.1. Chemicals:

In order to prepare the BTS_{11} ceramics, barium acetate $Ba(CH_3COO)_2$, titanium isopropoxide ($C_{12}H_{28}O_4Ti$) and tin chloride ($SnCl_2.2H_2O$) were used as raw materials, whereas acetic acid and 2-Methoxyethanol were used as the solvents. All reagents and solvents were of chemical grade were and used without any further purification.

2.2. Experimental methods:

The XRD patterns were obtained by X-ray diffraction using the Panalytical X-Pert Pro with Cu-Kα radiation (λ = 1.54059 Å) at room temperature ranging from 20° to 80°, while the surface morphology of the ceramic was examined using a scanning electron microscope (SEM, VEGA 3-Tescan). The density of the ceramic sample was determined by the Archimedes method. The micro-Raman Raman spectra were excited by the polarized radiation

of an argon laser with λ = 514 nm and were measured using a Renishaw in Via Reflex Raman spectrometer equipped with an Edge-filter. Temperature-dependent micro-Raman measurements were performed by aLinkam THMS600heating and freezing stage with a temperature stability of 0.1 K. The dielectric properties temperature dependence was measured using an impedance analyzer (HP 4284A) in the temperature range of 20to 80°C, and at frequency ranges of 20 Hz-100 kHz. Differential scanning calorimetry (Perkin Elmer Jade DSC) was used to point out the different phase transitions in a temperature range of -20 to 100°C. The polarization-electric field (P–E) hysteresis loops were performed by CPE1701, PloyK, USA, with a high voltage power supply (Trek 609-6, USA) in a silicone oil bath at 100 Hz in the temperature range of 5-120 °C. Finally, the electrocaloric study was carried out by the indirect method using the previously recorded P–E hysteresis loops. A silver paste was used to electrode the BTS_{11} ceramic pellet for the dielectric and ferroelectric measurements.

2.3. Synthesis procedure:

$BaTiSn_{11}$ ceramic was prepared via a sol-gel route. A suitable amount of barium acetate ($Ba(CH_3COO)_2$) was dissolved in glacial acetic acid, while tin chloride ($SnCl_2.2H_2O$) was dissolved separately in 2-methoxyethanol. The two solutions were then mixed at room temperature. The mixture was then stirred for 1 hour after a stoichiometric volume of titanium isopropoxide was added. The solution was then poured drop by drop with ammonia until it formed a clear gel, which was dried overnight before being calcined at 1000 °C for 4 hours. The resulted powder was then pressed under uniaxial compression in pellets of 8 mm diameter and 0.4mmthickness that were sintered at 1350°C for 7h.All chemicals are of analytical grade and used without further purification.

3. Results and discussion:

3.1. Structural and microstructural analysis:

The XRD of the BTS_{11} calcined powder and the sintered ceramic are displayed in figure 1(a, b).Both spectra show a pure perovskite structure with no heterogeneous peaks, indicating that Ti^{4+} has been completely replaced by Sn^{4+} in the BTS_{11} solid solution.The enlarged view of the calcined powder's 45° peak reveals a distinct splitting, indicating the presence of the tetragonal phase (Figure 1-c). The presence of the orthorhombic phase is indicated by the formation of a triplet at 65° (Figure 1-d)[18][19][20]. However, the enlarged viewsof the XRD peaks centred at 2θ=45° and 2θ=65° of the sintered BTS_{11} ceramicpresented in figure 1-e and figure 1-f respectively, indicate the presence of a single characteristic peak with a small shoulder towards lower angles. The merger of (200) and (002) peaks at 2θ=45°, and (202) and (220) peaks at 2θ=65° indicates the dominant cubic phase in the BTS_{11} ceramic at room temperature. Given the similarity of the total energies between the cubic phase (nonpolar phase) and the tetragonal, rhombohedral, and orthorhombic phases (polar phases), polar phases can be randomly generated, formed and embedded in the cubic phase matrix [21]. Thus, the Rietveld refinement of the dominant cubic phase with the space group Pm3m was performed using Fullprof suite software (figure 2-a).Table 1 compares the refined structural parameters of BTS_{11} ceramic at room temperature to those reported in the literature. As one can see in the table 1, the BTS_x ceramics exhibit different phase structures depending on the tin composition(x), usually the cubic phase is remarked when x exceeds 10%[13],[19],[17], and the tetragonal or the

orthorhombicphase is remarked when x takes a value below 10% [24],[25],[10]. Thus, a dominant phase of cubic is found in our BTS_{11} ceramic, which can be further demonstrated by Raman and DSC measurements.

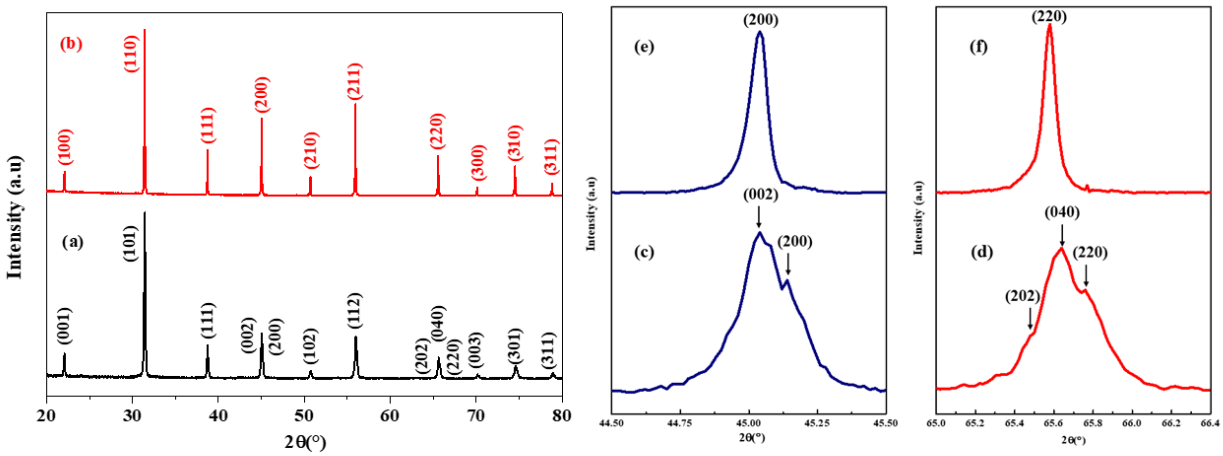

Fig.1 XRD patterns of (a) the calcined BTS_{11} powder and its the enlarged views of 45° XRD peak (c) and 65° peak (d), (b) XRD patterns of the sintered BTS_{11} ceramic, and its enlarged views of 45° XRD peak (e) and 65° peak (f).

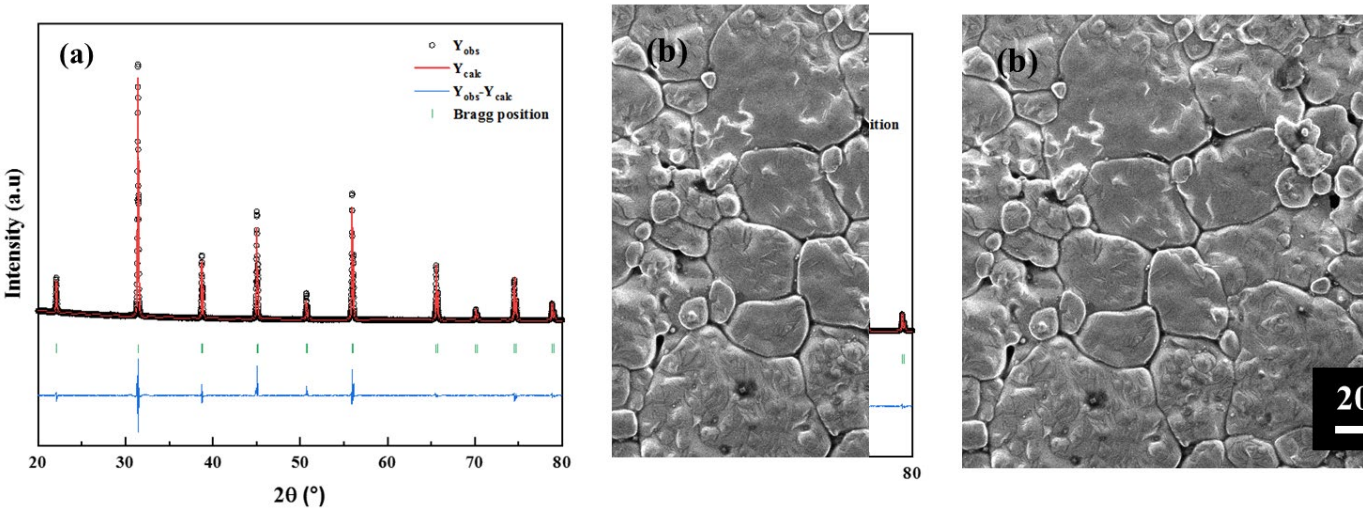

Fig.2 (a) Refined XRD patterns of the sintered BTS_{11} ceramic and (b) SEM micrograph the BTS_{11} sintered ceramic.

Table 1 Refined structural parameters for the BTS_{11} ceramic at room temperature in comparison with other BTS_xceramics.

Peparation method of BTS_x	Composition (x)	Structure	Calcination Temperature T°C/time (h)	Sintering temperature (°C) and time (h)	Cell volume($Å^3$)	Density	References
Sol-gel	11	Cubic *Pm-3m*	1000/4	1350/7	65.1224	5.91	This work
Low-temperature aqueous synthesis	13	Cubic	800/2	1300/2	-	-	[23]
Solid-state	5	Tetragonal *P4mm*	1130/2	1330/2	-	5.7	[24]
Solid-state	6.5	Orthorhombic *Amm2*	1050/4	1350/4	-	5.2	[25]
Solid state	10	Tetragonal *P4mm*	1100/4	1350/4	64.68	-	[10]
Sol-gel	20	Cubic	1000	1350/2	-	5.43	[17]
Solid state	12	Cubic	1100/2	1370/5	64.76	-	[22]

The SEM micrograph of the sintered BTS_{11} ceramic is presented in figure 2-b. The sintered ceramicexhibits coarse and large grains along with some smallparticles,resulting ina high density of 5.91g/cm^3 and an averagegrain distrubution of 18.5 µm.The small particles found in the BTS_{11} ceramic fill the gaps between the larger grains, improving densification and,eventualy,enhancing the dielectric and ferroelectric properties[26].

The DSC and the temperature dependence of Raman spectroscopy were performed for the BTS_{11}sintered ceramic to acquire more information about the phase transitions.

The DSC curve of our sample presented in figure 3-b shows a unique, small and large endothermic peak near ambient temperature between 28°C and 41°C.Indeed, as reported by Gao et al.[12], when the composition xof Sn dopant increases in BTS_x, the transition enthalpy atthe Curie temperature decreases gradually, and when it changes

to the multi-phase point (x=10.5), the heat flow peak becomes nearly invisible, indicating that first-order transition changes to the near second order. Thus, the presence of only one small endothermic peakindicates that the three phase transitions (T_{R-O}, T_{O-T} and T_{T-C}) are all overlapped in this large temperature range. Hence,due to the characteristics of the multi-phase boundary, highdielectric constant and ultra-high piezoelectric properties can be expectedin this temperature range [9,12].

Raman spercroscopy is a versatile method to probe the short range modes since itsstructural informations refers to a single TiO_6 octahedra, whereas the symmetry from XRD is due to a group of unit cells of more than 10 nm^3[27]. Thus, to confirm the multiphase co-existence in the BTS_{11}, the temperature dependence of Raman spectroscopy was performed and presented in figure 3-a.Note that at 0 °C, the spectral response contains the polar modes with E and A_1-symmetries typical for the tetragonal phase of the $BaTiO_3$ ceramics. Although the spectra change rather gradually with temperature, we observe several important features that are interpreted as the coexistence of different phases characteristic for the $BaTiO_3$ in a narrow temperature range. Below 30 °C, we note the presence of both bands$A_1(TO_1)$ at 150cm^{-1} and $A_1(TO_3)$ at 250cm^{-1},characteristic of the tetragonal and cubic symmetries.Moreover, the relative intensities of $E(TO_2)$ and $A_1(LO_2)$/E(LO) bands at 305 and 715 cm^{-1}, respectively, which are more intense below 30°C,indicate the presence of the tetragonal phase. The band at 190 cm^{-1} assigned to the orthorhombic phase is also visible up to 30°C[28]. Besides, the three modes $A_1(TO_1)$, $A_1(TO_3)$ and $E(TO_1)$ that identify the rhombohedral structure are also present up to 30°C. The disappearance of the characteristicmodes of all ferroelectric phases at 180cm^{-1} $A_1(TO_1)$, 305cm^{-1} $E(TO_2)$, and 715cm^{-1} $A_1(LO_2)$/E(LO) above 30°C confirms thatthe ferroelectric-paraelectric phase transition happens around this temperature. Thus, the BTS_{11} ceramic above 30°C startstransitinginto cubic paraelectric phase.

For additional support of the latter conclusion, the thermal variation of FWMH of the $A_1(TO_3)$ Raman mode has also been investigated and displayed in figure 3-b. This figure shows only one abrupt variation observed at a temperature range of 25-40°C, which can be associated with the three phase transitions, and confirmed the existence of the multiphase at near ambienttemperature[29].

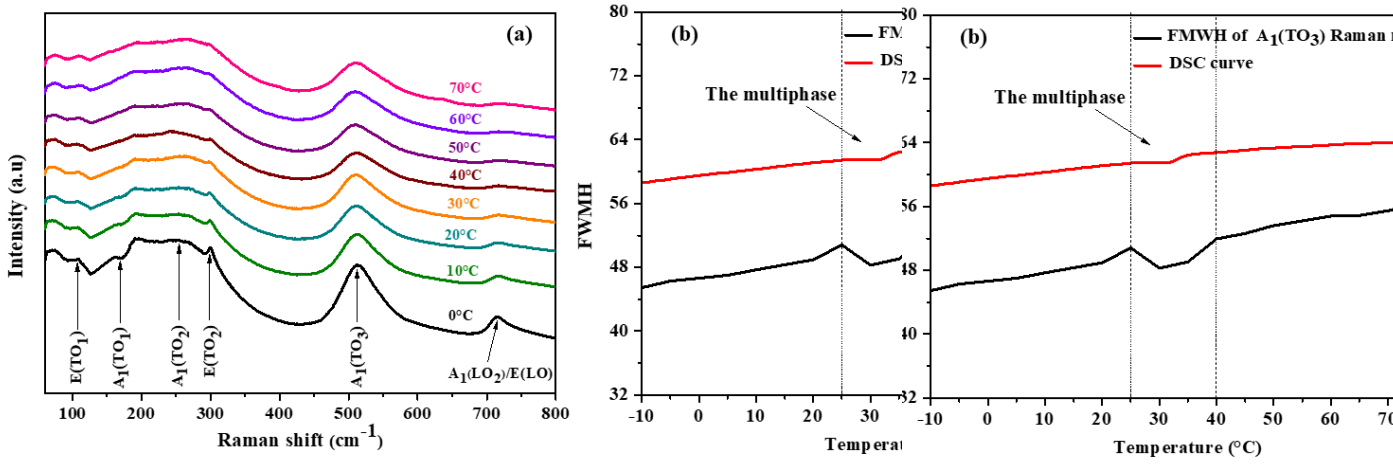

Fig.3 (a) Temperature dependence of Raman spectra (b) FWMH of the A1(TO3) Raman mode and the DSC curve of the sintered BTS_{11} ceramic.

3.2. Dielectric analysis

Figure 4 illustrates the temperature dependence of the dielectric constantε_r and the dielectric loss tanδ at various frequencies in the BTS_{11} sample from 20 to 80°C. For example, the dielectric constant at 1kHz reaches a maximum value of ε_{rmax}=15460 and a dielectric loss of tanδ=0.055 at the Curie temperature that happens to be at very nearambienttemperature (T_c=28°C) which is far less from the temperature reported in other works of BTS elaborated by the classicsolid-state method[30][31](Table2). The high value of ε_r may be due to the tricritical phenomenon occuring at the multi-phase point (x=11%) as well asthe elaboration method, the sol-gel method,which results in homogeneous powder particles and higher density BTS_{11} ceramic (Table 1).

The presence of only one anomaly, centered at 28 °C, suggests the existence of the multiphase (R-O-T-C) in the large temperature range of 20-42°C as predicted by the differential scanning calorimetry and the Raman spectroscopy.

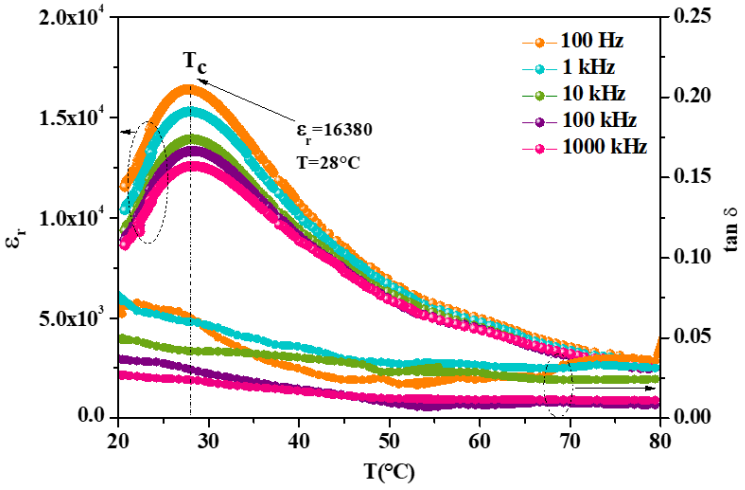

Fig.4 Temperature dependence of dielectric constant and the dielectric loss at various frequencies of the BTS_{11} ceramic sintered at 1350 °C / 7h.

The critical behavior of our BTS_{11} sample was quantified using the three equations below:

$$\frac{1}{\varepsilon_r} = \frac{T - T_0}{C} (T \succ T_0) \text{ (Eq.1)}$$

$$\Delta T_m = T_{dev} - T_m \text{ (Eq.2)}$$

$$\frac{1}{\varepsilon_r} - \frac{1}{\varepsilon_m} = \frac{(T - T_m)^\gamma}{C} (1 \prec \gamma \prec 2) \text{ (Eq. 3)}$$

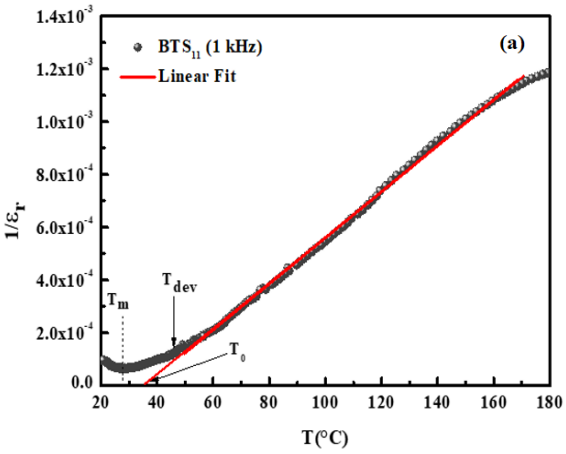

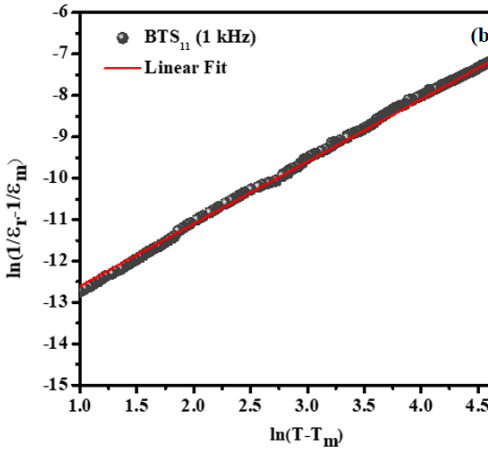

]

ceramic.

Where T_0 is the Curie temperature, C is the Curie-Weiss constant, ε_m is the maximum dielectric constant and T_m is the corresponding temperature, and γ is the degree of relaxation.

The degree of relaxation γ determines the type of the phase transition, it takes 1 as value when the material is a normal ferroelectric, and 2 when it is a relaxor, while it takes a value in between ($1<\gamma<2$) when there is the presence of an incomplete-diffused phase or relaxor-type phase transition[30,32]. The fitting results of the third equation (Eq.3) displayed in figure 5-b were used to quantify the value of the degree of relaxation. The summary of the dielectric results of our BTS_{11} is displayed in Table2 with a comparison of the dielectric properties at 1 kHz of other BTS_x ceramics. As we can see in Table 2, our BTS_{11} ceramic exhibits a high dielectric constant and a broad diffuse peak. In BTS_{11} and $BTS_{10.5}$ ceramics prepared by solid-state and reported S. by Merselmiz et al.[5] and Z. Luo [33] respectively, a high dielectric constants (17390) at T_m of 41 °C for BTS_{11} and (72000) at T_m of 28 °C for $BTS_{10.5}$ were reached. Those enhanced dielectric properties are explained by the fast thermodynamic energy provided by the presence of (C+R+T+O) multiple phase boundaries in the BTS ceramics. However, despite their high dielectric constant, sharp dielectric peaks were observed. The relaxation degree γ of our ceramic reached 1.428 which shows a rather broad (diffuse) dielectric constant peak compared to 1.34 reported by Merselmiz et al. [5] in a BTS_{11} elaborated by solid-state. However, M. Cernea et al, M. Kumari et al. and Md. J. Ansaree et al. reported important γ values of 1.536, 1.44 and 1.5 for a BTS_{13}, BTS_5 and BTS_{10} respectively but the dielectric constants were relatively low[23],[30],[34]. Hence, the enhanced dielectric properties found in our BTS_{11} ceramic synthesized by a sol-gel process is mainly due to the quasi quadruple point where all phases coexist.

Table3 Comparison of the dielectric properties at 1 kHz of the BTS_x ceramics.

Method	Composition (x)	ε_m	Tanδ	T_0 (°C)	$C\times10^5$ (K)	T_m (°C)	T_{dev} (°C)	ΔT_m (°C)	γ	References
Sol-gel	11	**15469**	0.055	36	1.15	**28**	45	32	**1.428**	This work

Solid-state	11	**17390**	0.055	51	1.44	**41**	80	39	**1,34**	[5]
Solid-state	10.5	**72000**	-	-	-	**28**	-	-	**-**	[33]
Sol-gel	10	2510	-	-	-	85	-	-	-	[17]
Low temperature aqueous synthesis	13	4800	0.23	-	-	31	-	-	1.536	[23]
Solid-state	5	4182	0.034	-	-	140	-	-	1.44	[30]
Solid-state	10	4610	-	-	-	-	-	-	1.5	[34]
	20	1296	-	-	-	-	-	-	2.01	
Solid-state	5	1230	0.055	81	1.48	77	-	2	1.1	[35]
Solid-state	10	5324	-	-	-	49	-	-	-	[31]

3.3. Ferroelectric properties and Energy storage performances:

The electric field dependent polarization performed at different temperatures from 10 to 100 °C under the applied field of 35kV/cm and a frequency of 100 Hz are shown in figure 6. The maximum value of the polarization (P_{max}=14.72µC/cm^2), the remanent polarization (P_r=2.99µC/cm^2), the charge storage density (Q_c=P_{max}-P_r =11.73µC/cm^2) and the coercive field (E_c= 1.01 kV/cm) of the BTS_{11} ceramic arefound near ambient temperature in the range of 10 to 40 °C. Meanwhile, the P-E hysteresis loop is observed to be slim and gets even slimmer with the increase of the temperature from 10 to 100 °C due to the ferroelectric-paraelectric phase transition. The ferroelectric behavior can be noticed in a broad temperature range, even above the Curie temperature (T_c=28°C) up to 60°C, due to the diffuse phase transition confirmed by the dielectric measurements.

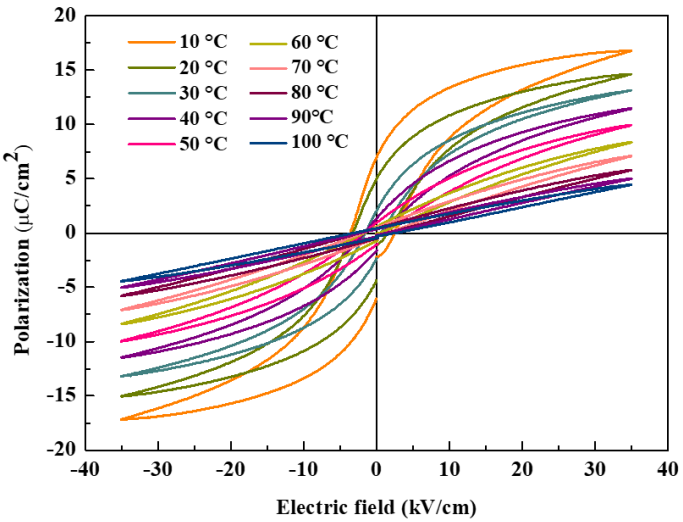

Fig.6 P-E hysteresis loops of the BTS_{11} ceramic from 10 °C to 100 °C.

The temperature-dependent variation of P_{max}, P_r, Q_c and E_c is shown in figure 7-a. P_{max} and P_r decrease with increasing the temperature due to the ferroelectric-paraelectric phase transition, whilst the coercive field takes a minimum value at 20°C, then stays approximately the same up to 80°C,after which it increases quickly with the increase of the temperature due to the conductive mechanism usually observed at high temperature and low frequencies [8].

The energy storage performance of the BTS_{11} ceramic was further investigated using three equations 4, 5 and 6. The total energy density W_{tot} was calculated by integrating the electric field from 0 to P_{max}, whilst the recovered energy density W_{rec} was determined fromthe integral of the electric field from P_r to P_{max}. Finally, the lost energy density W_{loss} was the difference between W_{tot} and W_{rec}.

$$W_{tot} = \int_0^{P_{max}} EdP \qquad \text{(Eq. 4)}$$

$$W_{rec} = \int_{P_r}^{P_{max}} EdP \quad \text{(Eq. 5)}$$

$$W_{loss} = W_{tot} - W_{rec} \quad \text{(Eq. 6)}$$

At ambient temperature, W_{tot}, W_{rec} and W_{loss} are169.8 mJ/cm^3, 110.3 mJ/cm^3, and 59.5mJ/cm^3, respectively. The thermal evolution of the energy storage properties is shown in figure 7-b. As we can observe from the figure, W_{tot} decreases with the temperature increase, whereas W_{rec} keeps an approximately constant value of 120 mJ/cm^3 in the temperature range of 30 °C-70 °C, and then it starts decreasing gradually with increasing temperature. It is worthy to note that the enhanced thermal stability in the BTS_{11} ceramic makes our quasi quadruple ferroelectric material a solid candidate for energy storage applications in a large temperature domain from the ambient to 80 °C [12].

The efficiency is also estimated using equation 7.

$$\eta(\%) = \frac{W_{rec}}{W_{tot}} \times 100 = \frac{W_{rec}}{W_{rec} + W_{loss}} \times 100 \quad (Eq.7)$$

The efficiency is a crucial parameter that helps determine the energy storage performance of the sample, as shown in figure 7-a. Initially, η increases quickly with increasing the temperature to78% at the ambient temperature (25 °C), then it increases very slowly to reach a maximum value of 84% at 60°C, and finally it starts decreasing gradually at 90 °C proving significant thermal stability of the BTS_{11} ceramic.

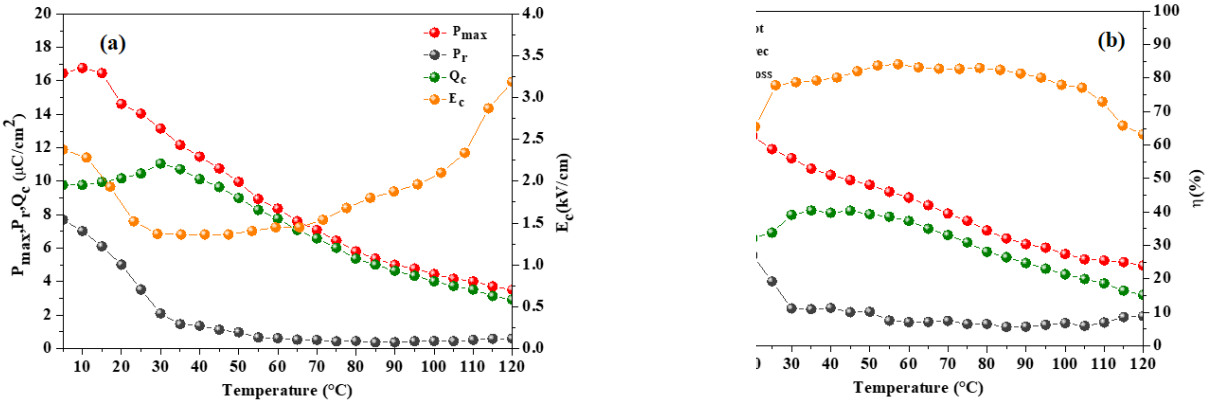

ceramic.

Table 3 sums up some energy storage properties of other barium titanate based ceramics. The results concerning the BTS, BST and BCZT ceramics reported in previous works (Table 3)are conducted under a high electric field and/or at high temperature, which is not a requirement for energy storage devices, the main goal is to obtain a slim hysteresis loop preferably at very near ambient temperature which is the case of our material, which makes it a good candidate for energy storage applications[12],[36],[5],[20].

Table 4 Comparison of the energy storage properties of our BTS_{11} ceramic with other barium titanate based ceramics.

Ceramic	Method	W_{tot} (mJ/cm³)	W_{rec} (mJ/cm³)	η (%)	E (kV/cm)	T (°C)	References
$BaTi_{0.89}Sn_{0.11}O_3$	Sol gel	151	117	78	35	30	This work
$BaTi_{0.89}Sn_{0.11}O_3$	Sol gel	104.9	71.3	67.9	25	28	This work
$BaTi_{0.895}Sn_{0.105}O_3$	Solid state	31	-	-	10	37	[12]
$BaTi_{0.89}Sn_{0.11}O_3$	Solid state	92.7	84.4	91.04	25	60	[5]

$Ba_{0.95}Ca_{0.05}Ti_{0.89}Sn_{0.11}O_3$	Sol-gel	208.83	107.25	51.36	31	30	[37]
$Ba_{0.4}Sr_{0.6}TiO_3$	oxalate co-precipitation	530	-	96.4	136	-	[38]
$Ba_{0.85}Ca_{0.15}Zr_{0.10}Ti_{0.90}O_3$	Solvothermal	-	14	80	6.5	120	[20]

3.4. Indirect electrocaloric measurements

The electrocaloric measurements in the BTS_{11} sample were done indirectly using the maxwell equation (Eq. 8), which exploits the hysteresis loops' thermal evolution.

$$\Delta T = -\int_{E_2}^{E_1} \frac{T}{\rho C_p}\left(\frac{\partial P}{\partial T}\right) E dT \quad \textit{(Eq. 8)}$$

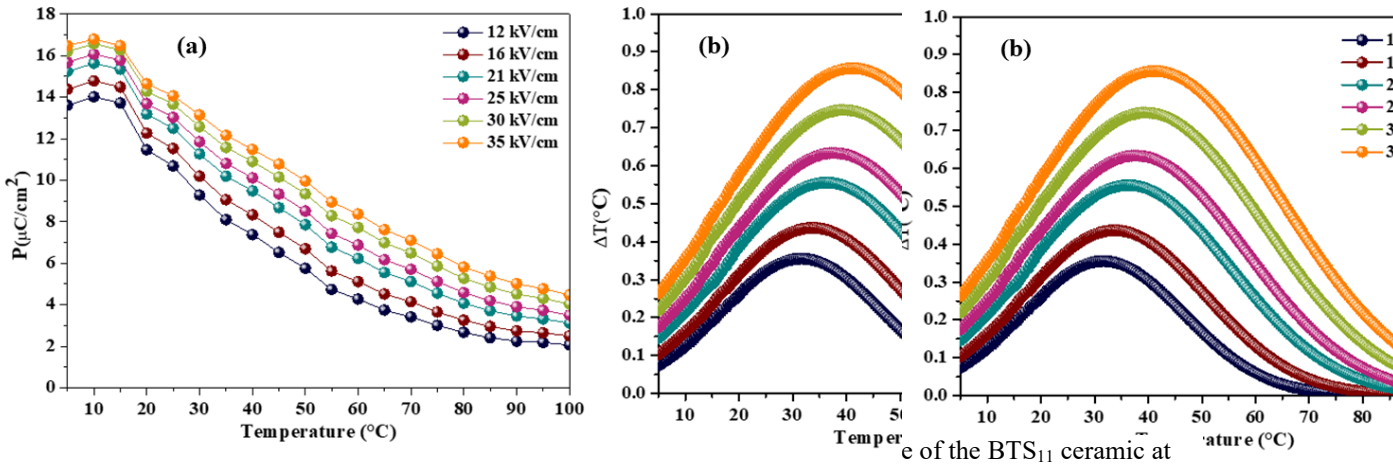

e of the BTS_{11} ceramic at different applied electric fields.

The evolution of the polarization P as a function of the temperature is shown in figure 8-a.P reaches a maximum value at 10 °C then decreases with a further increase in temperature due to the transition from the ferroelectric phase to the paraelectric phase, as previously mentioned. Figure 8-b depicts the thermal evolution of the adiabatic temperature of the BTS_{11} sample. The one thermally stable curve observed also confirms the existence of the multiphase as predicted by the DSC and Raman and confirmed by the dielectric measurements and shows the thermally stable electrocaloric performance in BTS_{11}. The maximum value of ΔT_{max} under 12 kV/cm is reached at30 °C, whereas under 35 kV/cm, ΔT_{max} is attained at 41 °C, which is commonly observed in ferroelectric materials[39].

The enhanced ΔT values of 0.86 and 0.64 K are obtained at 41 and 37 °C under 35 and 25 kV/cm respectively. As commonly reported in the literature, interesting electrocaloric response is usually observed at the quasi quadruple point where the total number of polar states is significant (12 polar states in an O phase, 8 polar states in a R phase,

and 6 polar states in a T phase),given that the entropy of an electrocaloric materiel depends on the total number of the polar states[39].Thus, in the quasi quadruple BTS reported in our work and also in the results reported by Z. Luo et al. [33], high adiabatic temperature is noticed under low electric field at low temperature. When the tin content is slightly below the quasi quadruple point (x<10.5), higher temperature is required to reach a high ΔT_{max}. For instance, in BTS_8 and BTS_{10} systems reported by W. Kayaphan et al. and S. Qiet al., a ΔT_{max} of 0.52 and 0.48Kwere reached under an applied field of 20 and 15 kV/cm at 58 and 64 °C respectively [40],[41]. Furthermore, H. Zaitouni et al. yielded an adiabatic temperature of 0.14 K in a BST system but at 108 °C [42], which is quiet comparable with what has been reported by H. Mezzourh et al. in the BCZT system[43]. Meanwhile, in $Ba_{0,95}Sr_{0,05}(Ti_{0,95}Zr_{0,05})_{0.75}Sn_{0.25}O_3$,ΔT reaches only 0.1 K under 10 kV/cm at 90 °C [44], and in $Ba_{0.85}Ca_{0.15}Ti_{0.90}Hf_{0.10}O_3$, the adiabatic temperature attains0.74Kunder 35 kV/cm but at high temperature (123°C) [45]. Therefore, the BTS_{11} is a promising ambient temperature electrocaloric material compared with other lead free system.

Furthermore, the electrocaloric responsivity ζ calculated by equation 9 (Figure 9) is used for further analysis of the electrocaloric behavior of the BTS_{11}ceramic. The maximum value of ζ (0.24K.mm/kV) is obtained at near ambient temperature, and its evolution as a function of the temperature in a broad temperature range is similar to the adiabatic temperature evolution. These results make our BTS_{11} material a potential candidate for practical near-ambient temperature frigorific applications.

$$\xi = \Delta T / \Delta E \quad \textit{(Eq. 9)}$$

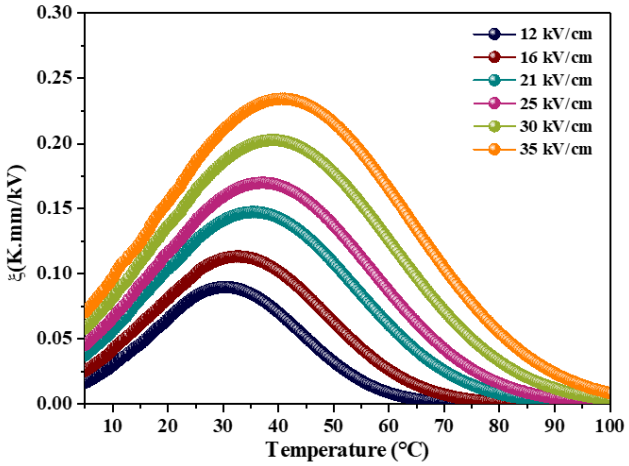

Fig.9 Temperature dependence ξ at different applied electric fields.

Table 4 summarizes the electrocaloric properties in our sample in comparison with similar and other lead-free materials at different applied electric field values.

Table5 Comparison of the electrocaloric properties of our BTS_{11} sample with other barium titanate based ceramics.

Ceramics	Method	T(°C)	ΔT_{max}(K)	ΔE (kV/cm)	ξ(K mm kV^{-1})	References
$BaTi_{0.89}Sn_{0.11}O_3$	Sol-gel	41	0.86	35	0.24	This work
$BaTi_{0.89}Sn_{0.11}O_3$	Sol-gel	37	0.64	25	0.17	This work
$BaTi_{0.895}Sn_{0.105}O_3$	Solid state	28	0.61	20	0.31	[33]
$BaTi_{0.92}Sn_{0.08}O_3$	Solid state	58	0.52	20	0.26	[40]
$BaTi_{0.9}Sn_{0.1}O_3$	Solid state	64	0.48	15	0.32	[41]
$Ba_{0.9}Sr_{0.1}TiO_3$	Semi wet	108	0.14	7	0.2	[42]
$Ba_{0.95}Ca_{0.05}Ti_{0.89}Sn_{0.11}O_3$	Sol-gel	62	0.807	30	0.268	[37]
$Ba_{0.85}Ca_{0.15}Zr_{0.10}Ti_{0.90}O_3$	Sol-gel	100	0.15	6	0.25	[43]
$0.7BaZr_{0.2}Ti_{0.8}O_3$– $0.3Ba_{0.7}Ca_{0.3}TiO_3$	Solid state	55	0.3	20	0.15	[46]
$Ba_{0,95}Sr_{0,05}(Ti_{0,95}Zr0,05)_{0.75}Sn_{0.25}O_3$	Solid state	101	0.095	10	0.095	[44]
$Ba_{0.85}Ca_{0.15}Ti_{0.90}Hf_{0.10}O_3$	Solid state	123	0.74	35	-	[45]

4. Conclusion

To summarize, we have investigated the structural, dielectric, ferroelectric, and energy storage and electrocaloric properties at very near ambient temperature in the eco-friendly BTS_{11} ceramic synthesized by the sol-gel method. As a result, a high dielectric constant of 15460, high recovered energy of 122 mJ/cm^3 with 79% efficiency and a significant electrocaloric effect (ΔT=0.86 K, ζ=0.24K.mm/kV under 35 kV/cm)are obtained near ambient temperature with remarkable thermal stability due to the overlap of the three phases transition. Hence, the BTS_{11} ceramic can be considered an excellent candidate for energy storage and frigorific applications near ambient temperature.

References:

1. Z. Surowiak, M. F. Kupriyanov, and D. Czekaj, J. Eur. Ceram. Soc. **21**, 1377 (2001).
2. A. R. James and K. Srinivas, Mater. Res. Bull. **34**, 1301 (1999).
3. D. A. Gidlow, Occup. Med. **65**, 348 (2015).
4. C. Zhao, Y. Huang, and J. Wu, InfoMat **2**, 1163 (2020).
5. S. Merselmiz, Z. Hanani, D. Mezzane, M. Spreitzer, A. Bradeško, D. Fabijan, D. Vengust, M. Amjoud, L. Hajji, Z. Abkhar, A. G. Razumnaya, B. Rožič, I. A. Luk'yanchuk, and Z. Kutnjak, Ceram. Int. **46**, 23867 (2020).
6. I. Coondoo, N. Panwar, D. Alikin, I. Bdikin, S. S. Islam, A. Turygin, V. Y. Shur, and A. L. Kholkin, Acta Mater. **155**, 331 (2018).
7. X. Wei and X. Yao, Mater. Sci. Eng. B **99**, 74 (2003).
8. L. Jin, J. Qiao, L. Hou, Y. Tian, Q. Hu, L. Wang, X. Lu, L. Zhang, H. Du, X. Wei, G. Liu, and Y. Yan, Ceram. Int. **44**, 21816 (2018).
9. Q. Zhao, H. Xiao, G. Huangfu, Z. Zheng, J. Wang, F. Wang, and Y. Guo, Nano Energy **85**, 106028 (2021).
10. W. Cai, Y. Fan, J. Gao, C. Fu, and X. Deng, J. Mater. Sci. Mater. Electron. **22**, 265 (2011).
11. J. Koruza, B. Rožič, G. Cordoyiannis, B. Malič, and Z. Kutnjak, Appl. Phys. Lett. **106**, 202905 (2015).
12. J. Gao, Y. Wang, Y. Liu, X. Hu, X. Ke, L. Zhong, Y. He, and X. Ren, Sci. Rep. **7**, 40916 (2017).
13. F. Guo, N. Jiang, B. Yang, and S. Zhao, Appl. Phys. Lett. **114**, 253901 (2019).
14. F. Guo, X. Wu, Q. Lu, and S. Zhao, Ceram. Int. **44**, 2803 (2018).
15. Z. Shi, Y. Liu, F. Guo, and S. Zhao, J. Mater. Sci. Mater. Electron. **32**, 12557 (2021).
16. S. Song, J. Zhai, L. Gao, X. Yao, S. Lu, and Z. Xu, J. Appl. Phys. **106**, 024104 (2009).
17. F. Du, B. Cui, H. Cheng, R. Niu, and Z. Chang, Mater. Res. Bull. **44**, 1930 (2009).
18. G. K. Sahoo and R. Mazumder, J. Mater. Sci. Mater. Electron. **25**, 3515 (2014).
19. D. S. Keeble, F. Benabdallah, P. A. Thomas, M. Maglione, and J. Kreisel, Appl. Phys. Lett. **102**, 092903 (2013).
20. Z. Hanani, D. Mezzane, M. Amjoud, A. G. Razumnaya, S. Fourcade, Y. Gagou, K. Hoummada, M. El Marssi, and M. Gouné, J. Mater. Sci. Mater. Electron. **30**, 6430 (2019).
21. D. Wang, Z. Fan, G. Rao, G. Wang, Y. Liu, C. Yuan, T. Ma, D. Li, X. Tan, Z. Lu, A. Feteira, S. Liu, C. Zhou, and S. Zhang, Nano Energy **76**, 104944 (2020).
22. S. Marković, M. Mitrić, N. Cvjetićanin, and D. Uskoković, J. Eur. Ceram. Soc. **27**, 505 (2007).
23. M. Cernea, R. Trusca, R. Radu, and C. Valsangiacom, J. Alloys Compd. **509**, 9934 (2011).
24. K. S. Srikanth, V. P. Singh, and R. Vaish, J. Eur. Ceram. Soc. **37**, 3943 (2017).
25. K. C. Singh, A. K. Nath, R. Laishram, and O. P. Thakur, J. Alloys Compd. **509**, 2597 (2011).
26. Z. Hanani, D. Mezzane, M. Amjoud, S. Fourcade, A. G. Razumnaya, I. A. Luk'yanchuk, and M. Gouné, Superlattices Microstruct. **127**, 109 (2019).
27. (n.d.).
28. A. Gajović, J. V. Pleština, K. Žagar, M. Plodinec, S. Šturm, and M. Čeh, J. Raman Spectrosc. **44**, 412 (2013).
29. L. P. Curecheriu, M. Deluca, Z. V. Mocanu, M. V. Pop, V. Nica, N. Horchidan, M. T. Buscaglia, V. Buscaglia, M. van Bael, A. Hardy, and L. Mitoseriu, Phase Transit. **86**, 703 (2013).
30. M. Kumari, N. Baraik, and P. M. Sarun, J. Alloys Compd. **883**, 160635 (2021).
31. H. C. R. Bitra and B. B. V. S. V. Prasad, Int. Lett. Chem. Phys. Astron. **32**, 191 (2014).

32. S. Hunpratub, S. Maensiri, and P. Chindaprasirt, Ceram. Int. **40**, 13025 (2014).
33. Z. Luo, D. Zhang, Y. Liu, D. Zhou, Y. Yao, C. Liu, B. Dkhil, X. Ren, and X. Lou, Appl. Phys. Lett. **105**, 102904 (2014).
34. Md. J. Ansaree, U. Kumar, and S. Upadhyay, Appl. Phys. A **123**, 432 (2017).
35. R. Kumar, I. Singh, R. Meena, K. Asokan, B. Birajdar, and S. Patnaik, Mater. Res. Bull. **123**, 110694 (2020).
36. Z. Song, H. Liu, M. T. Lanagan, S. Zhang, H. Hao, M. Cao, Z. Yao, Z. Fu, and K. Huang, J. Am. Ceram. Soc. **100**, 3550 (2017).
37. Y. Hadouch, S. Ben Moumen, H. Mezzourh, D. Mezzane, M. Amjoud, B. Asbani, A. G. Razumnaya, Y. Gagou, B. Rožič, Z. Kutnjak, and M. El Marssi, J. Mater. Sci. Mater. Electron. (2022).
38. (n.d.).
39. J. Li, J. Li, S. Qin, X. Su, L. Qiao, Y. Wang, T. Lookman, and Y. Bai, Phys. Rev. Appl. **11**, 044032 (2019).
40. W. Kayaphan and P. Bomlai, Adv. Mater. Sci. Eng. **2018**, 1 (2018).
41. S. Qi, G. Zhang, L. Duan, T. Zeng, and J. Cao, Mater. Res. Bull. **91**, 31 (2017).
42. H. Zaitouni, L. Hajji, D. Mezzane, E. Choukri, A. Alimoussa, S. Ben Moumen, B. Rožič, M. El Marssi, and Z. Kutnjak, Phys. B Condens. Matter **566**, 55 (2019).
43. H. Mezzourh, S. Belkhadir, D. Mezzane, M. Amjoud, E. Choukri, A. Lahmar, Y. Gagou, Z. Kutnjak, and M. El Marssi, Phys. B Condens. Matter **603**, 412760 (2021).
44. I. Djemel, I. Kriaa, N. Abdelmoula, and H. Khemakhem, J. Alloys Compd. **720**, 284 (2017).
45. X. Wang, J. Wu, B. Dkhil, C. Zhao, T. Li, W. Li, and X. Lou, RSC Adv. **7**, 5813 (2017).
46. Appl. Phys. Lett. **102**, 252904 (2013).